Desalination of Caspian Sea water by using graphene oxide-based covalent organic frameworks and HDTMA-modified Iranian natural Zeolite

Jahangir Abedi-Koupai[1], Arefeh Chehrehrazi[1], Fatemeh Dadvand[1], Mohammad Javad Amiri[2]*

[1]*Department of Water Science and Engineering, College of Agriculture, Isfahan University of Technology, Isfahan, Iran.*
[2]*Department of Water Engineering, Faculty of Agriculture, Fasa University, Fasa, Iran.*

***Corresponding author**: mj_amiri@fasau.ac.ir

Abstract:

The depletion of freshwater resources emphasizes the significance of water desalination, while the high energy consumption and operating costs associated with existing desalination methods necessitate the search for cost-effective solutions. Therefore, this study presents a unique and innovative solution by employing advanced materials, specifically the combination of graphene oxide (GO)-based covalent organic frameworks (COF) and hexadecyltrimethylammonium bromide (HDTMA)-modified Iranian natural zeolite in the desalination of Caspian Sea water and well water in the Dark area of Isfahan. In this regard, GO was synthesized using Homer's modified method and subsequently functionalized with COF and the clinoptilolite zeolite was modified with HDTMA. A series of 28 column experiments were carried out using response surface methodology (RSM) to examine the elimination of electrical conductivity (EC), sodium (Na^+), potassium (K^+), calcium (Ca^{2+}), magnesium (Mg^{2+}), and chloride (Cl^-) under the influence of five operational parameters: initial salinity ($7.3 - 9.6$ ds/m), flow rates ($1 - 5$ mL/min), GO amounts ($0 - 30$ mg), HDTMA quantities ($0 - 13$ g), and COF quantities ($0 - 30$ mg). The results revealed that the initial salinity concentration had the most significant impact on the reduction of EC, Na^+, K^+, and Mg^{2+}. Conversely, the quantities of COF had the greatest influence on the reduction of Ca^{2+}. Regarding Cl^-, the interaction between HDTMA and salinity exhibited the most notable effect. Overall, this study highlights the potential of utilizing GO and HDTMA-modified Iranian zeolite for desalination purposes, offering a promising approach for addressing water scarcity and salinity challenges in arid regions.

Keywords: Desalination; Graphene oxide; Iranian natural zeolite; HDTMA

1. Introduction

In arid and semi-arid regions, like the country of Iran, water scarcity is an unavoidable reality where limited water resources are contested by agricultural, domestic, and industrial demands. On the other hand, high levels of salinity in water can cause numerous issues across the three sectors of drinking, industry, and agriculture (Amiri et al. 2015; Banda et al. 2023). Consequently, the demand for desalination of brackish and seawater has dramatically increased to mitigate these challenges. The process of desalination involves removing dissolved salts and other minerals from brackish or seawater to render it suitable for human consumption

or industrial use (Aende et al. 2020). Several methods, including reverse osmosis, multi-stage flash, multi-effect distillation, electrodialysis, and ion exchange have garnered significant attention in desalination process (Abushawish et al. 2023). In light of the drawbacks and limitations associated with many existing methods, especially in the context of agricultural purpose, researchers are currently directing their focus towards the development of more cost-effective alternatives.

Adsorption is a highly practical and economically feasible method for removing a range of pollutants. These pollutants include heavy metals (Amiri et al. 2018; Rezaei-Aghdam et al. 2022), dyes (Bahrami et al. 2020), herbi-

Figure 1. Experimental setup for column tests.

cides (Amiri et al. 2020), chemical oxygen demand (COD), and total dissolved solids (TDS) (Amiri et al. 2019). This can be achieved by utilizing activated carbon (Amiri et al. 2019; Amiri et al. 2020) or other low-cost adsorbents such as agricultural wastes (Ungureanu et al. 2023), bio-apatite based materials (Amiri 2022), and zeolite (Amiri et al. 2019; Moghanjooghi et al. 2022). Graphene is often regarded as a "wonder material" due to its exceptional characteristics, such as high thermal and electrical conductivity, superior mechanical strength, and a significant specific surface area. The properties mentioned above make graphene and its derivatives highly attractive materials for a broad spectrum of applications, spanning from electronics and energy storage to biomedicine and environmental remediation (Yusaf et al. 2022; Joya-Cárdenas et al. 2022). The unique structure of GO grants it a high surface area and abundance of active sites, rendering it an efficient adsorbent for diverse pollutants, including heavy metals, organic compounds, and dyes (Sherlala et al. 2018; Mouhtady et al. 2022). Ongoing research is focused on enhancing the effectiveness and sustainability of GO for water purification applications. In addition, zeolites, which are crystalline aluminosilicates recognized for their unique attributes such as a substantial surface area, notable porous texture characteristics, and a high CEC (Solinska and Bajda 2022), have been effectively employed in various applications. These applications include the elimination of both organic and

inorganic contaminants (Amiri et al. 2019) as well as desalination processes (Wibowo et al. 2017; Sasani et al. 2021).

Rostamian et al., conducted a study on the utilization of biochar derived from rice husk for water desalination (Rostamian et al. 2015). The findings showed that raising the temperature during the production of biochar from 400 to 800°C had a beneficial impact on the structure by promoting the development of cavities and increasing its specific surface area. Wibowo et al., employed modified clinoptilolite zeolites as an adsorbent to reduce seawater salinity (Wibowo et al. 2017). Thermal activation at 225°C for 3 hours enhanced the adsorption capacity without the need for any reagents. The findings of the study demonstrated a significant salinity reduction of 4.8%, corresponding to 51.43 mg/g. Wan Azelee et al., successfully created a desalination membrane with exceptional permeability and selectivity by integrating a thin film layer that incorporates a hybrid material of multiwalled carbon nanotubes and titania nanotubes (MWCNT-TNT) for desalination (Azelee et al. 2017).

Wang et al. conducted a study to enhance the desalination performance of DUT-67 as a water-stable metal-organic framework (MOF), by incorporating varying amounts of GO to produce DUT-67/GO composites (Wang et al. 2023). The study found that the mesoporous structures present in composite materials are advantageous for efficient mass transportation. Out of all the composites tested, the DUT-67/GO with 24 wt% GO addition had the highest water

Table 1. Chemical analysis of used saline water.

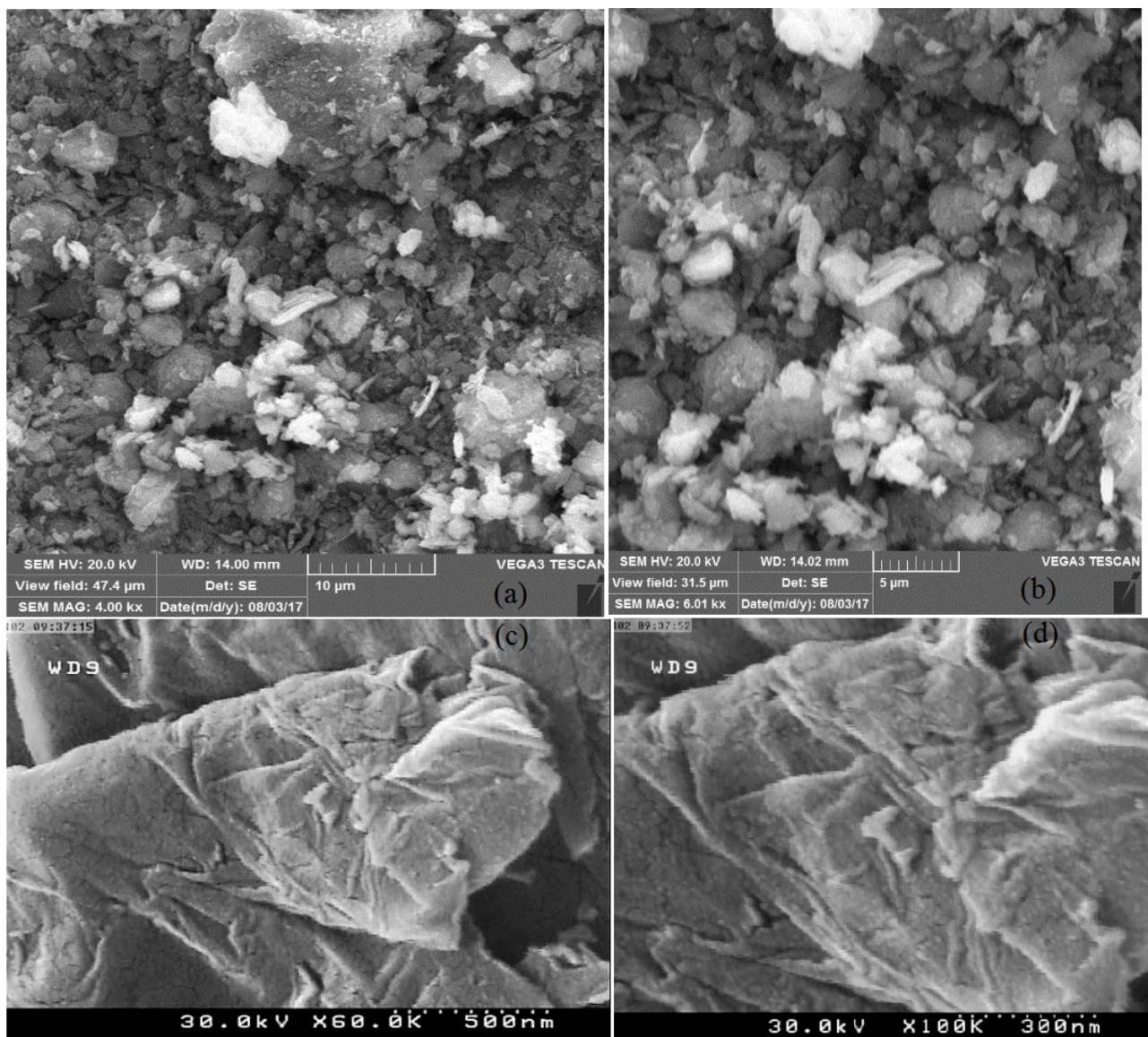| Source	Cl	HCO$_3$	CO$_3$	Mg	Ca	Na	P	pH	EC (dS/m)
				mg/L					
7.3	7.55	487.9	998.6	512	362.1	0	915	2275	Well water
9.6	7.85	1428.3	1312	384	622.1	0	1952	2765	Caspian Sea

Figure 2. SEM images of Iranian Natural Zeolite in (a) 10 μm, and (b) 5 μm; and synthesized GO in (c) 500 nm, and (d) 300 nm.

uptake and mass transfer coefficient. According to Lian et al., GO has a water uptake capacity of up to 0.58 g g^{-1}, which is significantly greater than that of silica gel (Lian et al. 2018). Zahed et al. conducted a study on the desalination of saline water using GO as an adsorbent (Zahed et al. 2018). They synthesized GO through both the Hummers and modified Hummers methods. The resulting GO was functionalized with chitosan. The study found that the modified Hummers method produced GO with a higher adsorption capacity for sodium ions than GO synthesized via the Hummers method. Furthermore, sodium adsorption capacity was improved upon functionalizing the GO with chitosan. Sadeghi et al. investigated the potential use of zeolite clinoptilolite for removing nitrate, phosphate, and salt from agricultural drainage water (Sadeghi et al. 2022). The study demonstrated that nitrate, phosphate, and salt ions were removed 63%, 39%, and 79%, respectively. Reverse osmosis is not a cost-effective method for desalinating saline water, particularly for the agriculture sector,

which is the largest water consumer in the world. This is due to the method' high energy requirements and associated costs, necessitating the use of alternative desalination methods. The GO and natural zeolite have been successfully examined for their effectiveness in adsorption dyes, nitrate, and heavy metals (Joya-Cárdenas et al. 2022; Mouhtady et al. 2022; Halouane et al. 2017; Wu et al. 2020). However, there is insufficient research on the capacity of these adsorbents for desalinating saline water. Therefore, this study offers a unique and innovative solution by utilizing advanced materials, specifically the combination of graphene oxide-based covalent organic frameworks (COFs) and hexadecyltrimethylammonium bromide (HDTMA)-modified Iranian natural zeolite, to address the challenge of desalinating water in arid and semi-arid regions. In this regard, RSM-CCD model was employed to optimize the effect of operational parameters in the desalination process using GO and modified Iranian natural zeolite on Caspian Sea water and Isfahan well water.
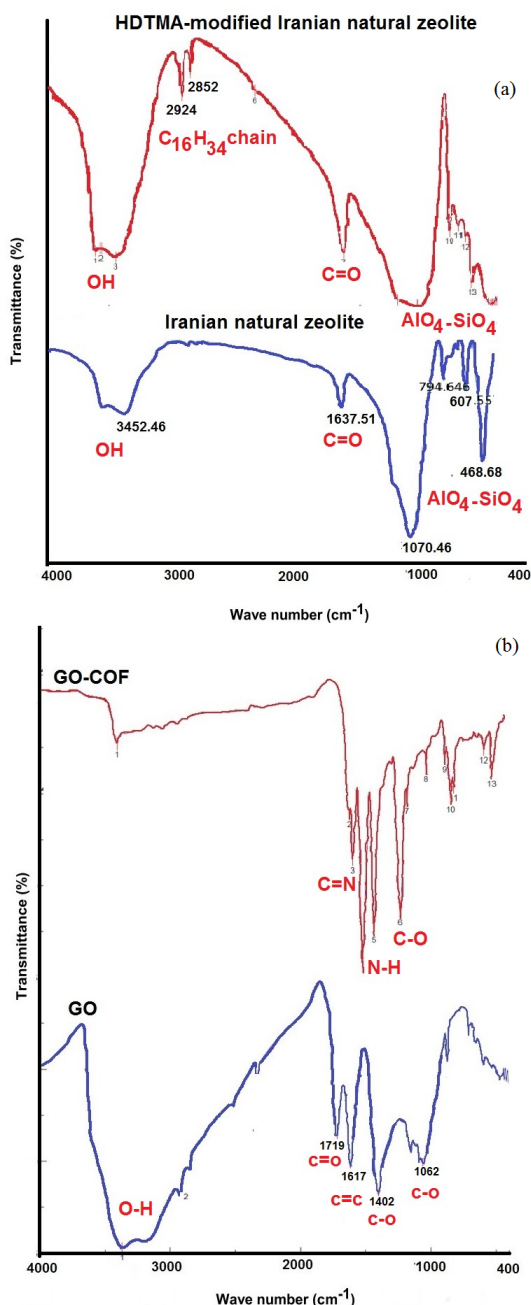
Figure 3. The FTIR spectra of (a) Iranian natural zeolite and HDTMA-modified Iranian natural zeolite, as well as (b) GO and GO-COF.

2. Material and methods

2.1 HDTMA-modified Iranian natural zeolite

In this study, clinoptilolite zeolite sourced from the Firoozkouh mine, located in the northeast of Firouzkooh township in Iran, was employed. The natural zeolite was subjected to multiple washes with boiling distilled water until the water passing through it became clear. Following that, it was dried in an oven overnight at 100°C . The resulting dried powder was then sieved to obtain a particle size of $0.5 - 0.8$ mm. The chemical composition of the Iranian clinoptilolite zeolite was obtained as follows (wt%): SiO_2 = 68.04; Al_2O_3 = 10.1; Fe_2O_3 = 2.05; TiO_2 = 0.42; CaO =

1.06; MgO = 1.35; Na_2O = 4.31; K_2O = 1.4; lost of ignition (LOI) = 10.82. The hexadecyltrimethylammonium bromide (HDTMA) surfactant is frequently employed for zeolite modification. The adsorption of HDTMA cations onto the zeolite surface occurs in different configurations, such as a monolayer, or double layer, depending on the surfactant concentration (Solinska and Bajda 2022). In previous studies, it has been established that a fully double-layered surfactant can be achieved when the ratio of adsorbed HDTMA to the external CEC of zeolite is 2:1 (equivalent to 200% ECEC) (Li and Bowman 1997). To determine the maximum ratio of salts adsorbed to HDTMA, the natural zeolite underwent various modifications using HDTMA at levels equivalent to 100, 150, 200, 250 and 300% of its ECEC. The ECEC of natural zeolite was found to be 70 mmol kg^{-1} according to Ming and Dixon (Ming and Dixon 1987). In this regard, a reciprocating shaker was used to mix 60 g of natural zeolite and 180 ml of 23, 35, 47, 58, and 70 mM HDTMA solution in 250-ml centrifuge bottle for a duration of 24 hours at 150 rpm. Afterwards, the mixture was subjected to centrifugation at 5000 rpm for a duration of 20 minutes. Subsequently, the concentration of the HDTMA solution in the supernatant was analyzed using an HPLC method. The targeted HDTMA treatment level was successfully achieved as evidenced by the constant equilibrium HDTMA concentration of 0.35 mM after reaching 200% of its ECEC.

2.2 Preparation of graphene oxide

Homer's modified method was used for the synthesis of graphene oxide, following the procedurea reported by Paulchamy et al. (Paulchamy et al. 2015). Briefly, 2 g of graphite and 2 g of sodium nitrate were mixed with 90 ml of sulfuric acid in an ice bath. Subsequently, 12 g of potassium permanganate was added gradually to the mixture, followed by the gradual addition of 184 ml of water. The ice bath was removed after a duration of 120 min, and the mixture was stirred for an additional 120 min at a temperature of 35°C. The mixture was then heated to 98°C and stirred for 120 min additional minutes after cooling to room temperature. Following treatment with 40 ml hy-
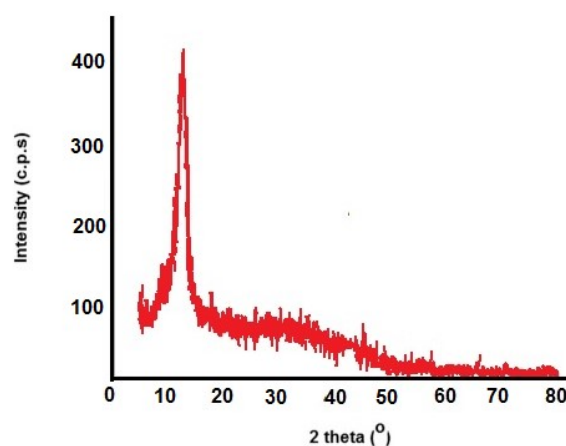

Figure 4. XRD analysis of GO.

Table 2. Experimental design for four independent variables and observed response rates for salinity parameters.

Response variable						Independent input parameters					
Cl	Mg	Ca	K	Na	EC	HDTMA+Z	COF	GO	Q	Salinity	No
mg/L	mg/L	mg/L	mg/L	mg/L	ds/m	g	mg	mg	mL/min	ds/m	.
700	142	208	333.24	-158.326	1.13	(0+13)	0	0	1	7.3	1
612.5	100	166	308.28	-104.386	1.09	(0+13)	0	0	5	7.3	2
787.5	151/6	212	358.1	-25.656	1.55	(0+13)	0	15	1	7.3	3
490	154	216	358.1	-25.656	1.1	(0+13)	0	15	5	7.3	4
787.5	113.2	176	407.46	25.594	1.6	(0+13)	0	30	1	7.3	5
700	127.6	180	407.46	99.714	1.32	(0+13)	0	30	5	7.3	6
595	186	134	1307.69	-73.034	1.88	(0+13)	0	0	1	9.6	7
490	156	104	1270.75	-36.294	1.61	(0+13)	0	0	5	9.6	8
560	165.6	120	1196.37	-36.297	1.27	(0+13)	0	15	1	9.6	9
577.5	132	100	1196.37	-36.297	1.07	(0+13)	0	15	5	9.6	10
525	182.4	132	1158.93	-0.004	1.58	(0+13)	0	30	1	9.6	11
455	144	104	1121.32	-0.004	1.34	(0+13)	0	30	5	9.6	12
1330	41	111	349.4	69.946	0.95	(0+13)	0	0	1	7.3	13
1312.5	34	104	323.77	21.978	0.9	(0+13)	0	0	5	7.3	14
1575	46.2	62	1182.17	283.473	2.25	(0+13)	0	0	1	9.6	15
1540	38.4	56	1144.09	221.157	2	(0+13)	0	0	5	9.6	16
980	68	141	401.37	21.978	0.97	(6.5+6.5)	0	0	1	7.3	17
962.5	65.2	136	375.26	-2.444	0.95	(6.5+6.5)	0	0	5	7.3	18
1277.5	109.2	79	1259.4	124.398	1.9	(6.5+6.5)	0	0	1	9.6	19
1190	103.2	72	1220.6	124.398	1.82	(6.5+6.5)	0	0	5	9.6	20
1050	58	156	323.77	93.492	1.35	(13+0)	0	15	1	7.3	21
1015	47	147	298.39	46.108	1	(13+0)	0	15	5	7.3	22
1225	70	156	323.77	162.378	1.74	(13+0)	0	30	1	7.3	23
1155	61	145	298.39	116.746	1.5	(13+0)	0	30	5	7.3	24
945	46	156	323.77	46.108	1.15	(13+0)	15	0	1	7.3	25
875	38	151	298.39	-2.444	1.05	(13+0)	15	0	5	7.3	26
1015	70	176	323.77	69.946	1.1	(13+0)	30	0	1	7.3	27
975	62	163	298.39	46.108	0.95	(13+0)	30	0	5	7.3	28

drogen peroxide, the mixture was washed with a solution of hydrochloric acid and deionized water. The resulting sediment was centrifuged and dried under vacuum at 25°C.

2.3 Graphene oxide-based covalent organic frameworks

To ensure better distribution of 1.5 g of GO in a 5 mL dioxane solvent, the mixture was placed in a 25 mL flask and subjected to ultrasonication for 30 minutes. This process not only facilitated the improved dispersion of GO
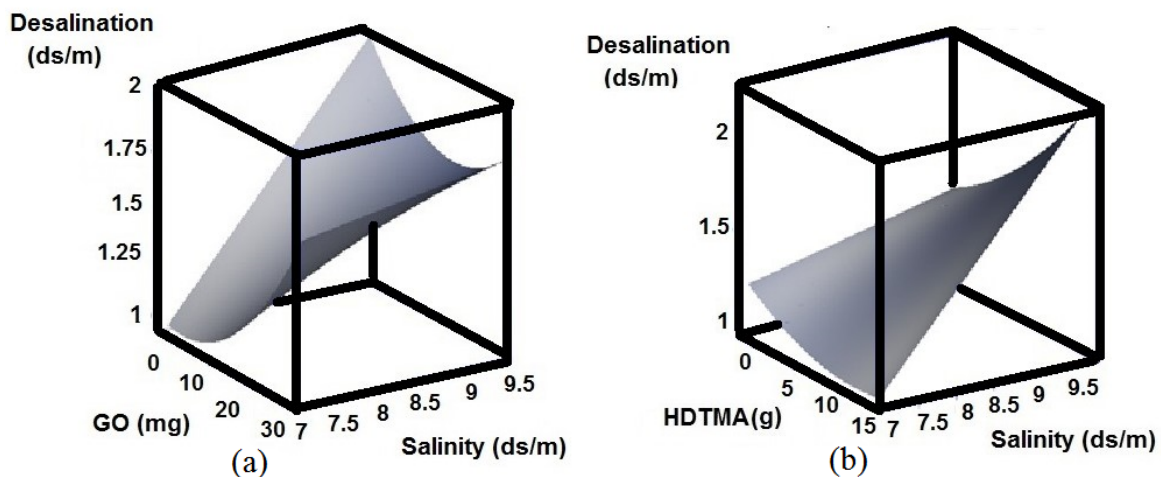

Figure 5. Surface plots for interaction of (a) GO∗Salinity and (b) HDTMA∗Salinity on Dsalination.

Table 3. Variance analysis of the response surface model for EC reduction capacity.

Parameter	P-value	t-value
Salinity	0.0044	3.5
GO	0.0243	2.58
COF	0.2842	1.12
HDTMA	0.0039	-3.56
Q	0.912	-0.11
GO×Salinity	0.0043	-3.51
GO×GO	0.0384	2.32
COF×COF	0.3333	-1.01
HDTMA×Salinity	0.0025	3.8
HDTMA×GO	0.1048	1.75
HDTMA×HDTMA	0.4516	0.78
Q×Salinity	0.8333	-0.22
Q×GO	0.2569	-1.19
Q×COF	0.9686	-0.04
Q×HDTMA	0.9507	0.06

throughout the solution but also enhanced the separation of individual GO sheets from one another. Simultaneously, a 0.136 g (0.74 mmol) amount of cyanuric chloride (CC) was dissolved in a 10 mL flask containing 2 mL of dioxane solvent. The resulting solution was then placed on a stirrer and maintained under nitrogen gas. Similarly, another 10 mL flask was prepared for the reaction. It contained 0.22 g (1.1 mmol) of 1,4-oxydianiline (ODA) and sodium hydroxide (0.088 g, 2.2 mmol of sodium hydroxide dissolved in 4 mL of deionized water). This flask was also placed on the stirrer under nitrogen gas. After a designated period, the dispersion of GO in dioxane solvent, along with the two other solutions prepared simultaneously, was combined and transferred into a 50 mL balloon. The balloon was sealed with nitrogen to maintain an inert atmosphere. The resulting mixture was then subjected to ultrasonication for 30 minutes, followed by stirring at room temperature for 6 hours. The reaction mixture was then filtered and subsequently dried under reduced pressure. The resulting precipitate was then washed multiple times using methanol and water. Finally, it was dried under vacuum conditions. The reaction product obtained is a white powder, exhibiting an efficiency of approximately 85% (Li et al. 2022; Zhang et al. 2022).

2.4 Concentration measurement

The concentrations of Sodium (Na^+) and potassium (K^+) were measured using a Flame Photometer (Corning 410, USA). The concentrations of calcium (Ca^{2+}), magnesium (Mg^{2+}), and chloride (Cl^-) were determined using the titration method and following standard analytical procedures (Greenberg et al. 1992). Additionally, the pH of the samples was measured using a pH meter (Metrohm, 827 pH Lab, Switzerland), while the electrical conductivity (EC) was measured using an EC meter (Hanna HI9835, USA).

2.5 Analytical techniques

The functional groups in adsorbents were investigated using a Jasco FT/IR-680 instrument (USA) within the range of

$400 - 4000\ cm^{-1}$ to determine their composition. To create the pellets, a mixture was prepared by combining 2% of the adsorbents (based on weight) with 100 mg of potassium bromide. The surface morphology of the adsorbents was examined using a SEM (TESCAN Vega 3, USA). Furthermore, the average pore size, and BET surface area of adsorbents were determined by conducting N_2 adsorption-desorption isotherms at a temperature of -196°C and a relative pressure of 0.98. These measurements were carried out using a Bel-sorp mini II instrument (Japan).

2.6 Data analysis

Two methods exist for studying and optimizing the influence of operational factors in the adsorption process. The first method is known as "one-variable-at-a-time," which can be a time-consuming and expensive task. In this method, the user must sequentially change one variable factor while keeping the other factors constant. The second one, known as the multivariable statistical method, is utilized for the optimization of the operational factors (Bahrami et al. 2020; Amiri 2022). In order to optimize the removal of salts from both Caspian Sea water and well water in the dark area of Isfahan, RSM-CCD model was utilized using MINITAB version 16 software. RSM-CCD is a powerful approach that can be employed to examine the interrelationships and cooperative properties among significant parameters at various levels. In the RSM-CCD model, the experimental data were subjected to regression analysis to fit them into a second-order polynomial equation.

$$y = b_0 + \sum_{i=1}^{k} b_i x_i + \sum_{i=1}^{k} b_{ii} x_{ii}^2 + \sum_{i=1}^{k} \sum_{j=i+1}^{k} b_{ij} x_i x_j + \varepsilon \quad (1)$$

In this Eq, the predicted response is denoted by y, whereas x_i and x_j represent the independent factors. The constant coefficient is represented by b_0, and the regression coefficients for linear, quadratic, and interaction effects are represented by b_i, b_{ii}, and b_{ij}. The statistical error is denoted by ε, and k represents the number of patterns.

Table 4. Variance analysis of the response surface model for sodium reduction.

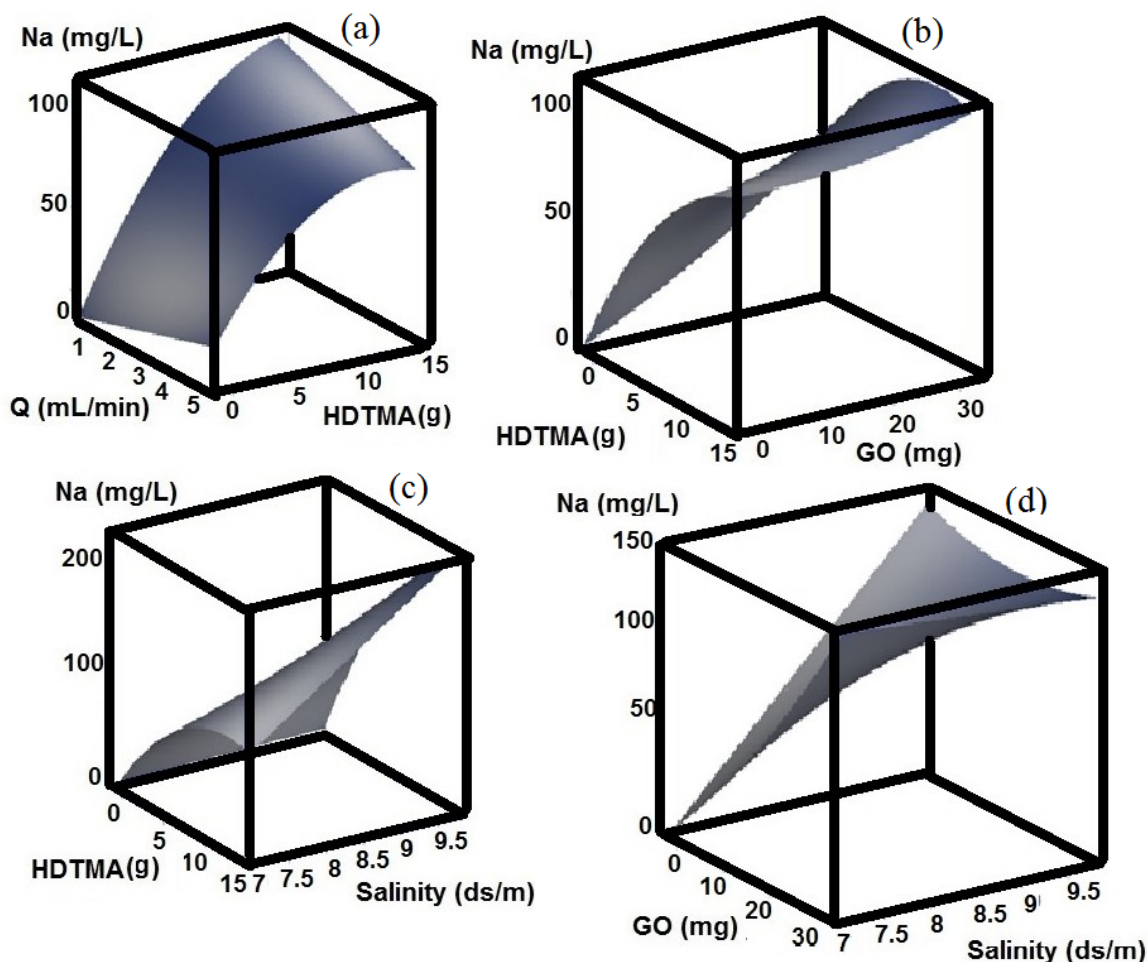| Parameter	P-value	t-value
Salinity	0.0017	4.04
GO	0.0001	6.01
COF	0.0913	-1.84
HDTMA	0.5665	-0.59
Q	0.1548	1.52
GO×Salinity	0.0001	-5.49
GO×GO	0.3505	0.97
COF×COF	0.071	1.98
HDTMA×Salinity	0.0001	5.97
HDTMA×GO	0.0016	-4.04
HDTMA×HDTMA	0.0035	-3.63
Q×Salinity	0.3031	-1.08
Q×GO	0.8466	-0.2
Q×COF	0.5358	0.64
Q×HDTMA	0.0003	-5.06

Figure 6. Surface plots for interaction of (a) Q∗HDTMA; (b) HDTMA∗GO; (c) HDTMA∗Salinity; and (d) GO∗Salinity; on Na$^+$ reduction.

2.7 Saline water samples

To simulate natural conditions, we utilized water from two distinct sources: the Caspian Sea and a well located in the dark area of Isfahan. These sources were chosen due to their varying concentrations of salinity, cations, and anions. Table 1 presents the chemical analysis results for the waters employed in this study.

2.8 Dynamic adsorption experiments

For the column test, a piston with an inner diameter of 1.5 cm and a height of 13 cm was utilized. The piston serves as a means to control the movement and flow of the fluid within the column during the experiment. A porous sheet was employed to seal the bottom of the column, ensuring that only water could exit while effectively preventing the adsorbent material from escaping the column. To create the first type of column, we evenly distributed 13 g of either natural zeolite or its modified form inside the column, effectively filling a height of 7 cm. To construct the second type of column, we prepared a pack consisting of two layers of filter paper. Each layer contains either 15 or 30 mg of GO or its modified form. Then, the prepared pack was inserted into the column, with 5.6 g of zeolite-based material positioned at the bottom of the pack, followed by 6.5 g of zeolite

placed above it. This arrangement ensures proper layering within the column. The saline water was introduced into the column in a downward direction using peristaltic pump (Miclins, India) with a consistent flow rate of either 1 or 5 mL min^{-1} as shown in Figure 1. This uniform flow rate ensures that the water passes through the column steadily and consistently during the adsorption process. Finally, the desired ion concentration in the solution that passes through the column can be measured using standard methods.

3. Results

3.1 Characterization

Based on Figures 2a and 2b, it can be observed that Iranian clinoptilolite zeolite exhibits a morphology characterized by the presence of coarse particles with irregular shapes and sizes. SEM images effectively illustrate the unevenness and roughness observed in the zeolite particles, attributable to their crystalline structure and the presence of diverse surface features. According to Figures 2c and 2d, the surfaces of GO exhibit a relatively smooth appearance with minimal roughness. The smoothness is attributed to the presence of oxygen-containing functional groups introduced through the oxidation process, which enhances the hydrophilicity and results in a smoother surface compared to pristine graphene

Table 5. Variance analysis of the response surface model for potassium reduction.

Parameter	P-value	t-value
Salinity	0.0001	6.68
GO	0.0001	10.07
COF	0.0626	-2.05
HDTMA	0.0001	8.43
Q	0.5117	0.68
GO×Salinity	0.0001	-12.38
GO×GO	0.0606	2.07
COF×COF	0.1789	1.43
HDTMA×Salinity	0.0001	-7.93
HDTMA×GO	0.0001	-6.02
HDTMA×HDTMA	0.0007	-4.55
Q×Salinity	0.2425	-1.23
Q×GO	0.5281	0.65
Q×COF	0.832	0.22
Q×HDTMA	0.2663	-1.17

(Sherlala et al. 2018; Mouhtady et al. 2022). Figure 3a displays the FTIR spectra of the Iranian clinoptilolite zeolite in its pristine state, and after modification with HDTMA. The presence of two peaks at about $3600 - 3400$ cm^{-1} can be attributed to the OH stretching vibrations of molecular water (Solinska and Bajda 2022). Within the $1100 - 460$ cm^{-1} spectral region, the observed bands corresponded to the vibrations of AlO$_4$ and SiO$_4$, which are indicative of the zeolite framework (Solinska and Bajda 2022). Upon modification, the FTIR spectra exhibited the emergence of two distinct peaks at 2924 cm^{-1} and 2852 cm^{-1}. These peaks can be attributed to the asymmetric and symmetric stretching vibrations, respectively, of the hexadecyl chain of HDTMA (Guan et al. 2010). The observed shift in the peak positions can be associated with an increase in the disorder of the hexadecyl group of the surfactant molecules. This increase in disorder may result from the incomplete saturation of the zeolite's surface by HDTMA (Guan et al. 2010). Figure 3b depicts the FTIR spectra of the GO before and after functionalization with organic-covalent frameworks. The FTIR spectra of the prepared GO demonstrate successful functionalization with various oxygen-containing functional groups. The spectra confirm the presence of the C-O bond in the alkoxy group (1062 cm^{-1}), while the band observed at 1402 cm^{-1} indicates the stretching specifically associated with the C-O bond in the epoxy groups. The stretching vibration bands corresponding to the C=C bond in unoxidized carbons are observed in the region of 1617 cm^{-1}, while the C=O bond of the carboxyl group is observed in the region of 1719 cm^{-1}. A distinct peak at 3368 cm^{-1} is observed, indicating the presence of hydroxyl groups (O-H) attributed to water molecules (Sherlala et al. 2018). The successful grafting of the triazine polymer network onto the GO sheets has been thoroughly documented by the FTIR analysis, as shown in Figure 3b. The stretching band observed in the region of $1602 - 1577$ cm^{-1} is a distinct characteristic of the C=N bond, as clearly depicted in the Figure. This observation provides strong confirmation of the incorporation of

triazine groups into the polymer structure on the surface of GO. The stretching vibration band corresponding to the N-H bond is observed in the region of 1577 cm^{-1}, while the C-O bond is observed in the region of 1213 cm^{-1}. The absence of a strong and wide band in the region of $3500 - 2500$ cm^{-1} can be attributed to the formation of an ester group resulting from the bond between cyanuric chloride and the carboxylic acid groups. Additionally, the band observed in the region of 3387 cm^{-1} is one of the distinctive characteristics of the N-H group, specifically of the first type (Li et al. 2022; Zhang et al. 2022; Zaefizadeh et al. 2011). The BET surface area and average pore diameter of Iranian clinoptilolite zeolite were found to be 15.9 m2/g and 19.4 nm, respectively. In contrast, GO exhibited values of 48.4 m2/g for surface area and 5.1 nm for average pore diameter. The XRD analysis of GO as shown in Figure 4 reveals a distinct peak at $2\theta = 10 - 12°$, suggesting the existence of a well-organized structure. The amorphous nature of GO is confirmed by the absence of sharp diffraction peaks in its XRD pattern.

3.2 Maximizing desalination capacity through optimization of adsorbent composition

The maximum desalination capacity was achieved by utilizing a RSM-CCD test plan. Four independent input parameters that influenced the response variable, namely the amount of zeolite (Z) and zeolite modified with a HDTMA (13 g of zeolite or 13 g of HDTMA-modified zeolite, or 5.6 g of zeolite and 5.6 g of HDTMA-modified zeolite), initial salinity of the passing water (7.3 and 9.6 ds/m), inlet flow rate (Q) (1 and 5 mL/min), amount of GO (15 and 30 mg), and the amount of graphene oxide functionalized with a covalent organic framework (COF) (15 and 30 mg), were selected. A total of six response variables were taken into consideration, which included the concentrations of Na$^+$, K$^+$, Ca^{2+}, Mg^{2+}, Cl$^-$, and EC in the drainage water. The experimental design is presented in Table 2.

Table 6. Variance analysis of the response surface model for calcium reduction.

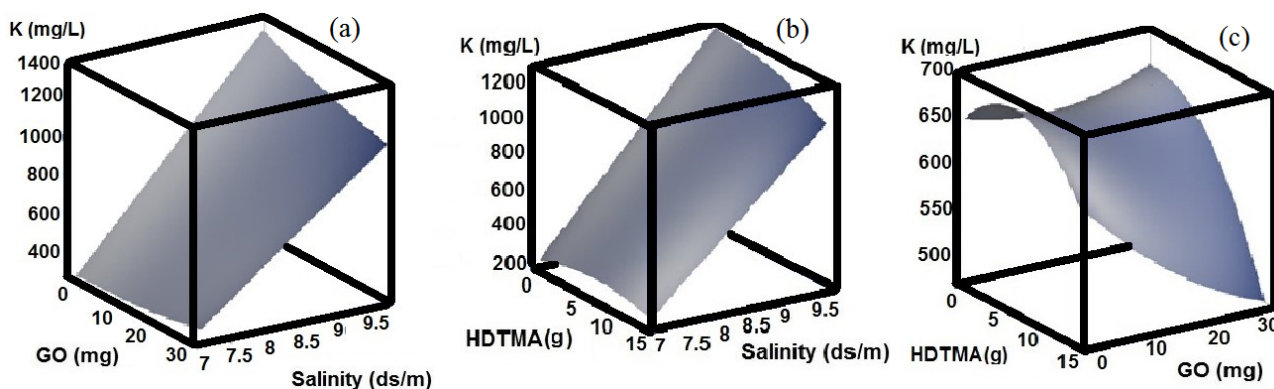| Parameter	P-value	t-value
Salinity	0.0001	-5.48
GO	0.7176	0.37
COF	0.0281	2.5
HDTMA	0.0073	-3.23
Q	0.9613	0.05
GO×Salinity	0.7013	0.39
GO×GO	0.0367	-2.35
COF×COF	0.2308	-1.26
HDTMA×Salinity	0.1041	1.76
HDTMA×GO	0.0153	2.82
HDTMA×HDTMA	0.1882	1.4
Q×Salinity	0.5973	-0.54
Q×GO	0.6553	0.46
Q×COF	0.817	-0.24
Q×HDTMA	0.3961	0.88

Figure 7. Surface plots for interaction of (a) GO∗Salinity; (b) HDTMA∗Salinity; and (c) HDTMA∗GO; on K^+ reduction.

3.3 EC

The RSM-CCD model demonstrated a high determination coefficient of 93.9%, indicating a strong correlation between the response and independent variables. Additionally, the P-value of 0.0001 further highlights the model's significance in expressing this relationship, as it is well below the threshold of 0.05. The analysis of variance (ANOVA) was employed to analyze the results, as presented in Table 3. Based on the P-values for each variable in Table 4, it indicates that a quadratic relationship has been established between the response and the significant variables. The adequacy of RSM-CCD fits is indicated by a large t-value, whereas the significance of the regression coefficients is demonstrated by p-values lower than 0.05 (Amiri 2022). The relationship between the reduction in EC and the corresponding independent variables is outlined below:

$$EC = -0.38 + 0.22S - 0.21Z + 0.064 \cdot G + 0.007G^2 - 0.009GS + 0.023SZ \tag{2}$$

In this case, the primary salinity variable of the passing water is represented by the letter S (measured in dS/m), the flow variable is denoted by the letter Q (measured in mL/min), the graphene oxide variable is indicated by the letter G (measured in mg), the functionalized graphene oxide variable is represented by the letter C (measured in mg), and the amounts of HDTMA is denoted by the letter Z (measured in g). The significance of the regression model values was assessed using the p-value. A negative sign in Eq. 2 denotes an antagonistic effect of the variables, suggesting that an increase in these factors will lead to a decrease in EC. Furthermore, a positive sign indicates a synergistic effect, suggesting that an increase in these factors will result in an increase in EC. Based on this relationship and the coefficients associated with each variable, it can be concluded that the initial salinity of the passing water has the most pronounced positive effect on desalination. Furthermore, increasing the amount of HDTMA while decreasing the amount of zeolite results in a reduction in the extent of desalination.

Three-dimensional surface plots were utilized, as demonstrated in Figure 5, to visualize the manifestation of responses at different levels of independent variables. When the amount of GO is increased in lower initial salinity, desalination improves. However, in higher initial salinities, a higher quantity of GO adsorbent has a negative effect on desalination (Figure 5a). Figure 5b shows that as the initial salinity of the incoming water increases, the amount of desalination also increases. Furthermore, as the concentration of HDTMA-modified zeolite increases at lower initial salinity, the level of desalination decreases; conversely, at higher initial salinity, the degree of desalination increases.

3.4 Na$^+$

Na$^+$ is the primary cation responsible for water salinity, and its high concentration is the most significant factor that restricts the utilization of saline water resources. Table 4 presents an analysis of the capacity of zeolite and GO, as well as their modified forms with HDTMA and COF to adsorb sodium. The coefficient of determination was calculated to be 98.47%, and the P-value was determined to be 0.0001 (< 0.05), highlighting the significant relationship between the response variable and the independent variables, thus emphasizing the significance of the model. Based on the P-values provided in Table 4 for each variable, a quadratic relationship has been established between the response variable and the significant variables. The following equation describes the relationship between the amount of sodium reduction and the effective independent variables.

$$Na^+ = 389.15 + 32.77S + 19.04G - 1.88GS + 4.66SZ - 0.257ZG - 0.92Z^2 - 1.62QZ \tag{3}$$

To examine the impact of independent variables on sodium reduction, three-dimensional surface plots were generated by varying two parameters while keeping the other three parameters constant. Figure 6a illustrates that sodium adsorption decreases as the flow rate increases. Moreover, an increase in the amount of HDTMA leads to an increase in sodium adsorption. The interactive effect of GO and HDTMA-modified zeolite on the removal efficiency of sodium is shown in Figure 6b. At lower amounts of HDTMA, the sodium concentration decreases with an increase in GO. However, as the amount of HDTMA reaches its optimum value, the impact of GO diminishes, and its effect becomes negligible. As illustrated in Figure 6c, increasing the amount of HDTMA up to 6.5 g, in conjunction

Table 7. Variance analysis of the response surface model for magnesium reduction.

Parameter	P-value	t-value
Salinity	0.017	2.77
GO	0.4703	0.75
COF	0.9259	0.09
HDTMA	0.6313	-0.49
Q	0.667	0.44
GO×Salinity	0.5365	-0.64
GO×GO	0.5134	-0.67
COF×COF	0.5987	0.54
HDTMA×Salinity	0.2516	-1.2
HDTMA×GO	0.2411	1.23
HDTMA×HDTMA	0.5265	0.65
Q×Salinity	0.3958	-0.88
Q×GO	0.7846	0.28
Q×COF	0.8745	-0.16
Q×HDTMA	0.5009	0.69

with a rising salinity concentration, led to an enhancement in the removal of Na^+ ions. Figure 6d indicates that at lower salinity levels, there is a decrease in sodium concentration with an increase in GO. However, as the salinity level increases, the influence of GO diminishes.

3.5 K^+

Table 5 illustrates the potassium adsorption capability of zeolite, GO, and their modified forms. The coefficient of determination was found to be 99.96%, indicating a high degree of correlation. Additionally, the P-value was calculated to be 0.0001 (< 0.05), emphasizing the model's significance in capturing the relationship between the response between the response variable and the independent variables. By considering the P-values presented in Table 5 for each variable, a quadratic relationship has been established. The following equation describes this relationship, expressing the amount of potassium adsorption in relation to the effective independent variables:

$$K^+ = -2713.42 + 418.34S + 23.94G + 47.21Z - \\ 3.19GS - 4.66SZ - 0.287ZG - 0.869Z^2 \quad (4)$$

According to Table 5, only three input factors, namely initial salinity, the amounts of GO and HDTMA, are found to be significant and can impact the levels of potassium in the effluent water.

Figures 7a and 7b demonstrate that as the initial salinity of the incoming water increases, the amount of potassium adsorption also increases. However, the influence of GO and HDTMA on the reduction of potassium is diminished at high initial water salinity. Conversely, at low initial salinity, an increase in GO and HDTMA up to 12 mg and 6.5 g, respectively, leads to an increase in potassium adsorption. However, further increases in these adsorbents have an adverse effect on potassium reduction. In other words, beyond a certain threshold, increasing the quantity of GO and HDTMA-Z may result in a diminishing or even negative impact on the reduction of potassium. This suggests that there

is an optimal dosage range for these adsorbents where their effectiveness in reducing potassium concentration is maximized. Beyond that range, increasing the amount of GO and HDTMA may not yield the desired results and could potentially hinder the reduction process. Figure 7c demonstrates that both GO and HDTMA-Z exhibit significant reductions in potassium concentration. However, HDTMA-Z outperforms GO in terms of its effectiveness in potassium reduction. HDTMA-Z possesses a layered structure with intercalated surfactant molecules. This structure provides an advantageous environment for the adsorption of potassium ions between the layers, facilitating stronger and more efficient binding. On the other hand, GO has a relatively flat and less organized structure, limiting its ability to accommodate potassium ions with the same level of effectiveness.

3.6 Ca^{2+}

Calcium is a prevalent element found in the majority of natural waters, and its concentration is influenced by the geological composition of the areas it traverses. As a result, the water in the Dark region of Isfahan contains a significantly higher amount of calcium compared to the water in the Caspian Sea. This discrepancy can be attributed to the types of rock formations present in each region, which directly affect the calcium content in the respective water sources. Table 6 evaluates the calcium adsorption capabilities of zeolite, GO, and their modified forms. The model's determination coefficient was 95.95%, indicating a strong ability to explain the relationship between the response and independent variables. Additionally, the associated P-value of 0.0001, which is less than the significance level of 0.05, further highlights the statistical significance of the model. Based on the P-values presented in Table 6, a quadratic relationship has been established between the response variable and the significant independent variables. The following equation depicts the relationship between the amount of

Table 8. Variance analysis of the response surface model for chlorine reduction.

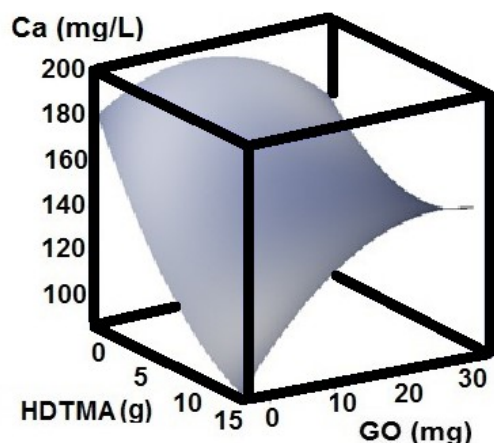| Parameter	P-value	t-value
Salinity	0.0361	-0.7
GO	0.3766	0.92
COF	0.0057	-3.36
HDTMA	0.0421	-0.57
Q	0.3651	-0.94
GO×Salinity	0.1311	-1.62
GO×GO	0.1269	1.64
COF×COF	0.0163	2.79
HDTMA×Salinity	0.0093	3.1
HDTMA×GO	0.1074	-1.74
HDTMA×HDTMA	0.0427	-1.53
Q×Salinity	0.5416	0.63
Q×GO	0.9999	0
Q×COF	0.9946	0.01
Q×HDTMA	0.3829	0.91

Figure 8. Surface plots for interaction of HDTMA∗GO on Ca^{++} reduction.

calcium reduction and the influential independent variables:

$$Ca^{++} = 445.61 - 32.98S + 3.99C - 17.84Z - 0.067G^2 + 0.133ZG \tag{5}$$

Table 6 reveals that three input factors, namely initial salinity, the amounts of COF and HDTMA, have been identified as significant in determining the levels of calcium in the effluent water. The analysis indicates that COF (covalent organic framework) exhibits a synergistic effect on calcium reduction, meaning that an increase in the amount of COF leads to a greater reduction in calcium levels in the effluent water. On the other hand, both HDTMA and salinity demonstrate an antagonistic effect on calcium reduction. This implies that higher levels of HDTMA or salinity can hinder or reduce the effectiveness of calcium reduction, resulting in lower reductions in calcium concentration in the effluent water.

According to Table 6, the interaction effect between HDTMA and GO has been identified as the only factor with a significant impact on calcium reduction. This suggests that the combined presence or interaction between HDTMA and GO influences the reduction of calcium levels in the system. The underlying mechanisms for this interaction could be attributed to various factors. HDTMA-Z and GO may have complementary adsorption characteristics or surface properties, leading to improved calcium adsorption capacity when used together. Additionally, the interaction between HDTMA-Z and GO may create a more favorable environment or enhanced binding sites for calcium ions, facilitating their removal from the system. As illustrated in Figure 8, an increase in GO concentration coupled with a decrease in HDTMA concentration leads to an enhancement in calcium reduction. Indeed, the zeolite adsorbent without surfactant demonstrates better performance in removing calcium from saltwater.

3.7 Mg^{2+}

Table 7 presents data on the adsorption capacity of magnesium using different materials, including zeolite, graphene

oxide, and their modified forms. The model used to analyze these relationships yielded a determination coefficient of 95.05% and a P-value of 0.0001 (< 0.05). These statistical results highlight the significance of the RSM-CCD in effectively expressing the relationship between the response variable and the independent variables. According to Table 7, the individual and interaction effects of the input parameters, except for initial salinity, did not exhibit a significant impact on magnesium reduction. This implies that the variations in these parameters, both individually and in combination, did not result in significant changes in the reduction of magnesium levels. However, the findings indicate that there is a positive correlation between the initial salinity of the input water and the adsorption of magnesium. Higher salinity corresponds to an increase in the concentration of dissolved ions in the water. This increased ionic strength can enhance the electrostatic attraction between magnesium ions and the adsorbent material, thereby promoting greater magnesium absorption.

3.8 Cl^-

Table 8 presents the adsorption capacities of chlorine by various materials, including zeolite, GO, HDTMA-modified zeolite, and COF-modified GO. The RSM-CCD used in the analysis achieved a determination coefficient of 96.67% and a P-value of 0.0001 (< 0.05), indicating the model's significance in expressing the relationship between the response variable and independent variables. The statistical analysis of Table 8 suggests that a quadratic relationship has been established between the chlorine reduction and the significant independent variables as follows:

$$Cl^- = 943.23 - 36.69C - 28.85S - 21.36Z + 0.941C^2 - 1.96Z^2 + 12.26ZC \tag{6}$$

As illustrated in Figure 9a, increasing the amount of HDTMA up to 6.5 g, in conjunction with a rising salinity concentration, led to an enhancement in the removal of Cl^- ions. As depicted in Figure 9b, by increasing the amount of COF from 0 to 15 g, there was a decrease in the removal of chlorine. However, with a further increase in the amount of COF from 15 to 30 g, the amount of chlorine removal increased. This Figure also indicates that the rate of chlorine removal remains unchanged with an increase in the flow rate.

4. Discussion

The objective of this study was to assess the performance of a combination of GO-based COF and HDTMA-modified Iranian natural zeolite as an innovative approach to address the challenge of desalinating water from the Caspian Sea and well water in the Dark area of Isfahan. The column, which comprised 13 g of HDTAM-modified zeolite and 30 mg of GO, exhibited the highest desalination capacity of 23.84% for well water in the Dark region of Isfahan. Likewise, for Caspian Sea water, the highest desalination capacity of 23.43% was achieved utilizing 13 g of HDTAM-modified zeolite. According to the findings of Xu et al. it
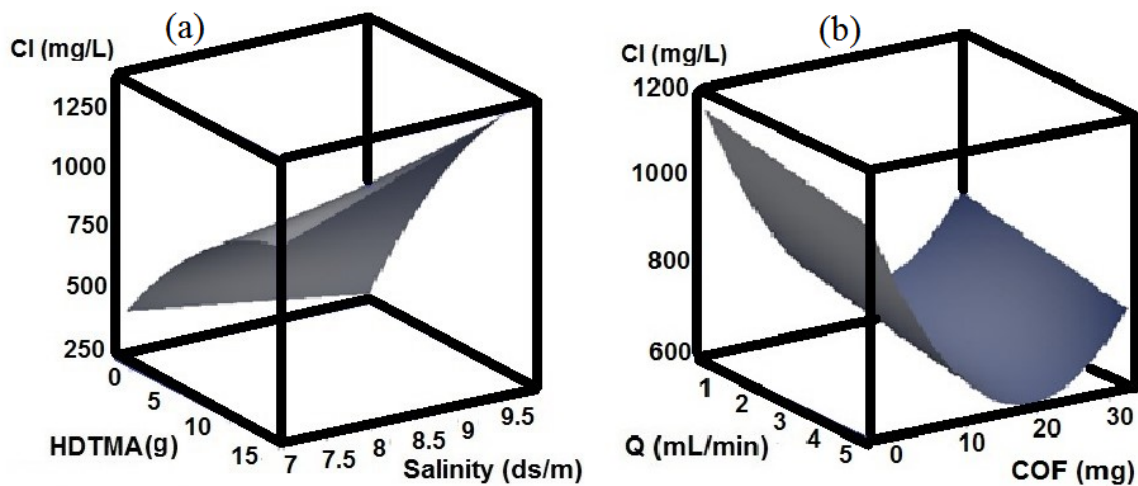
Figure 9. Surface plots for interaction of (a) HDTMA*Salinity and (b) COF*Q on chlorine reduction.

was observed that the presence of negatively charged surface functional groups on GO facilitated the desalination of water (Xu et al. 2020). In a separate study conducted by Nguyen and Beskok (Nguyen and Beskok 2019), it was demonstrated that charged nanoporous graphene membranes possess significant potential in reverse osmosis desalination systems, leading to improved performance. Paul et al. demonstrated that the utilization of acid-treated and Ca(OH)$_2$-conditioned natural zeolites has proven to be an effective method for filtering sodium ions from saline water and potash brine-spiked groundwater (Paul et al. 2017). In a study conducted by Sadeghi et al., the potential application of zeolite clinoptilolite for the removal of nitrate, phosphate, and salt from agricultural drainage water was investigated (Sadeghi et al. 2022). The findings of the study revealed that nitrate, phosphate, and salt ions were successfully removed by 63%, 39%, and 79%, respectively.

Calcium and magnesium are crucial elements for plant growth and are prevalent in natural systems. The calcium-to-magnesium ratio is a significant parameter used to assess the quality of irrigation water. When the calcium-to-magnesium ratio drops below one, particularly in saline conditions, it negatively impacts the physical and chemical properties of the soil. This imbalance disrupts the nutritional equilibrium, leading to a decline in plant performance (Filippi et al. 2021). The repeated occurrence of droughts and excessive exploitation of groundwater resources have resulted in a significant decline in both water level and quality. This decline includes a pronounced increase in salinity levels and, in certain cases, a relative rise in the concentration of magnesium ions. In the Dark area of Isfahan, the calcium-to-magnesium ratio is greater than one, indicating a lower risk of magnesium-imbalanced soil. However, it is important to note that the calcium content in the water of this area exceeds the permissible limit. On the other hand, in Caspian Sea water, the calcium-to-magnesium ratio is less than one. This implies that utilizing this water for agriculture without proper desalination measures is not feasible due to the unfavorable ratio for crop growth (Filippi et al. 2021). The highest calcium reduction of 84.37% for well water was achieved by combining 13 g of zeolite with 15 mg of GO.

Similarly, for Caspian Sea water, the utilization of 13 g of zeolite resulted in a calcium reduction rate of 69.79%. In the case of well water, employing 13 g of zeolite led to the highest magnesium reduction rate of 79.41%. Likewise, for Caspian Sea water, the highest magnesium reduction rate of 60.54% was obtained using 13 g of zeolite. Aghakhani et al. examined the effectiveness of various combinations of peat, activated carbon, zeolite, anionic resin, and cationic resin in removing salinity ions from aqueous media (Aghakhani et al. 2011). The study findings confirmed that the use of cationic resin resulted in higher desalination ability of the drainage water compared to anionic resin. Furthermore, the combination of cationic resin with peat was determined to be the most effective choice.

Desalination using HDTMA-modified Iranian natural zeolite can be categorized into three steps: (1) adsorption; HDTMA modification enhances the adsorption capacity of natural zeolite by introducing hydrophobic properties. (2) ion exchange; the HDTMA cations present on the surface of the zeolite attract and undergo an exchange process with the ions in the saline solution. (3) diffusion; the movement of ions from saline water to the zeolite surface occurs through a diffusion process. The desalination mechanism of GO-COF primarily relies on two key steps: adsorption and ion transport. The functional groups present on the GO-COF surface facilitate the adsorption of ions through electrostatic interactions and other binding forces. Furthermore, within the framework of GO-COF, a transport mechanism takes place, allowing ions to move through the interconnected pores and channels present in the material's structure.

To compare the operation costs of GO-based COF and HDTMA-modified Iranian natural zeolite, several factors need to be considered. These factors include the cost of starting materials, synthesis or modification processes, energy consumption, and any additional operational expenses. GO can be relatively expensive, depending on the source and quality. The synthesis of COF generally involves multiple steps and may require specific reagents, which can contribute to the overall cost. The energy required for synthesis and any subsequent activation processes should be considered. Operational expenses may include maintenance

or replacement costs for the system, which necessitates an investigation into adsorbent recovery and regeneration. On the other hand, natural zeolite is generally more cost-effective when compared to GO. The cost of modifying zeolite with HDTMA will depend on the reagents used and any additional treatments required.

5. Conclusions

This research successfully identified an optimal column configuration by utilizing graphene oxide and zeolite adsorbents as well as their modified forms, for efficiently removing cations and anions responsible for salinity. The results indicated that increasing the flow rate from 1 mL/min to 5 mL/min generally resulted in reduced desalination. Conversely, an increase in the initial salinity of the incoming water led to an increase in the degree of desalination. The column consisting of 13 g of zeolite modified with HDTAM and 30 mg of GO achieved the highest desalination capacity of 23.84% for well water in the Dark region of Isfahan. Similarly, for Caspian Sea water, the highest desalination capacity of 23.43% was obtained using 13 g of zeolite modified with HDTAM. The combination of 13 g of zeolite modified with HDTAM and 30 mg of GO achieved the highest sodium reduction of 16.22% for well water. Similarly, for Caspian Sea water, the highest sodium reduction of 21.57% was obtained using 13 g of zeolite modified with HDTAM. The combination of 13 g of zeolite and 15 mg of GO achieved the highest calcium reduction of 84.37% for well water. Similarly, for Caspian Sea water, the highest calcium reduction of 69.79% was obtained using 13 g of zeolite. In the case of well water, the utilization of 13 g of zeolite resulted in the highest magnesium reduction rate of 79.41%. Likewise, for Caspian Sea water, employing 13 g of zeolite led to the highest magnesium reduction rate of 60.54%. The highest chlorine reduction rates of 58.46% and 56.96% were achieved for well water and Caspian Sea water, respectively, by utilizing 13 g of zeolite modified with HDTAM. The combination of 13 g of zeolite and 30 mg of GO resulted in the highest potassium reduction rate of 83.51% for well water. Similarly, the column consisting of 13 g of zeolite achieved the highest potassium reduction rate of 91.5% for Caspian Sea water. The combination of both low-cost and high-cost materials offers the potential to not only reduce the price of desalination but also increase the adsorption capacity of the final product. This approach offers the advantage of achieving cost-effectiveness while simultaneously enhancing the efficiency of desalination processes. However, the main limitations and challenges of the study include the high cost associated with the production and utilization of graphene oxide-based COF, the long-term stability and durability of adsorbents, decreased performance due to variations in water chemistry and composition, as well as the lack of practical implementation and large-scale desalination.

Conflict of interest statement:
The authors declare that they have no conflict of interest, regarding the publication of this manuscript.

Author Contributions:
Conceptualization, J.A-K; writing—original draft preparation, A.C.; F.D.; M.J.A.; writing—review and editing, M.J.A.; supervision, J.A-K. All authors have read and agreed to the published version of the manuscript.

References

Abushawish A, Bouaziz I, Almanassra IW, AL-Rajabi MM, Jaber L, Khalil AKA, Takriff MS, et al. (2023) Desalination pretreatment technologies: current status and future developments. *Water* 15:1572.

Aende A, Gardy J, Hassanpour A (2020) Seawater Desalination: a review of forward osmosis technique, its challenges, and future prospects. *Processes* 8:901.

Aghakhani A, Mousavi SF, Mostafazadeh-Fard B, Rostamian R, Seraji M (2011) Application of some combined adsorbents to remove salinity parameters from drainage water. *Desalination* 257:217–223.

Amiri MJ (2022) Synthesis and optimization of spherical nZVI (20-60 nm) immobilized in bio-apatite-based material for efficient removal of phosphate: Box-Behnken design in a fixed-bed column. *Environ. Sci. Pollut. Res.* 29:67751–67764.

Amiri MJ, Arshadi M, Giannakopoulos E, Kalavrouziotis IK (2018) Removal of mercury (II) and lead (II) from aqueous media by using a green adsorbent: Kinetics, thermodynamic, and mechanism studies. *J Hazard Toxic Radioact Waste* 22:04017026.

Amiri MJ, Bahrami M, Kalavrouziotis M Badkouby IK (2019) Greywater treatment using single and combined adsorbents for landscape irrigation. *Environ. Process.* 6:43–63.

Amiri MJ, Eslamian S, Arshadi M, Khozaei M (2015) Water recycling and community. In: Eslamian, S. (Ed.) Urban water reuse handbook. 261–273. CRC Press

Amiri MJ, Roohi R, Arshadi M, Abbaspourrad A (2020) 2,4-D adsorption from agricultural subsurface drainage by canola stalk-derived activated carbon: Insight into the adsorption kinetics models under batch and column conditions. *Environ. Sci. Pollut.Res.* 27:16983–16997.

Azelee I Wan, Goh PS, Lau WJ, Ismail AF, Rezaei-DashtArzhandi M, Wong KC, Subramaniam MN (2017) Enhanced desalination of polyamide thin film nanocomposite incorporated with acid treated multi-walled carbon nanotube-titania nanotube hybrid. *Desalination* 409:163–170.

Bahrami M, Amiri MJ, Bagheri F (2020) Optimization of crystal violet adsorption by chemically modified potato starch using response surface methodology. *Pollution* 6:159–170.

Banda H, Rezk A, Elsayed E, Askalany A (2023) Experimental and computational study on utilising graphene oxide for adsorption cooling and water desalination. *Appl. Therm. Eng.* 229:120631.

Filippi FM De, Iacurto S, Grelle G, Sappa G (2021) Magnesium as environmental tracer for karst spring baseflow/overflow assessment—a case study of the Pertuso karst spring (Latium region, Italy). *Water* 13:93.

Greenberg AE, Clasceri LS, Eaton AD (1992) Standard Methods for the Examination of Water and Wastewater. American Public Health Association, American Water Works Association and Water Pollution Control Federation, Washington, DC. *J Envi Manag* 238:119–25.

Guan H, Bestland E, Zhu Ch, Zhu H, Albertsdottir D, Hutson J, Simmons CT, Ginic-Markovic M, Tao X, Ellis AV (2010) Variation in performance of surfactant loading and resulting nitrate removal among four selected natural zeolites. *J. Hazard Mater.* 183:616–621.

Halouane F, Oz Y, Meziane D, Barras A, Juraszek J, Singh SK, Kurungot S, et al. (2017) Magnetic reduced graphene oxide loaded hydrogels: Highly versatile and efficient adsorbents for dyes and selective Cr (VI) ions removal. *J. Colloid Interface Sci.* 507:360–369.

Joya-Cárdenas DR, Rodríguez-Caicedo JP, Gallegos-Muñoz A, Zanor GA, Caycedo-García MS, Damian-Ascencio CE, Saldaña-Robles A (2022) Graphene-based adsorbents for arsenic, fluoride, and chromium adsorption: synthesis methods review. *Nanomaterials* 12:3942.

Li Y, Xu X, Guo H, Bian Y, Li J, Zhang F (2022) Magnetic graphene oxide-based covalent organic frameworks as novel adsorbent for extraction and separation of triazine herbicides from fruit and vegetable samples. *Analytica Chimica Acta* 1219:339984.

Li ZH, Bowman RS (1997) Counterion effects on the sorption of cationic surfactant and chromate on natural clinoptilolite. *Environ. Sci. Technol.* 31 (8): 2407–2412.

Lian B, Luca SD, You Y, Alwarappan S, Yoshimura M, Yoshimura V, Smith SC, Leslie G, Joshi RK (2018) Extraordinary water adsorption characteristics of graphene oxide. *Chem. Sci.* 9:5106.

Ming DW, Dixon JB (1987) Quantitative determination of clinoptilolite in soils by a cation-exchange capacity method. *Clay, Clay Miner.* 35 (6): 463–468.

Moghanjooghi S Mousavi, Khoramnejadian Sh, Fataei E, Monsan AA (2022) Effect of various insectides on Pseudaulacaspis pentagona and its parasitoied on Kiwifruit trees (Actinidia chinensis). *Journal of Novel Researches on Plant Protection* 5 (1): 44–35.

Mouhtady O, Obeid E, Abu-samha M, Younes K, Murshid N (2022) Evaluation of the adsorption efficiency of graphene oxide hydrogels in wastewater dye removal: application of principal component analysis. *Gels.* 8:447.

Nguyen CT, Beskok A (2019) Charged nanoporous graphene membranes for water desalination. *Phys. Chem. Chem. Phys.* 21:9483–9494.

Paul B, Dynes J, Chang W (2017) Modified zeolite adsorbents for the remediation of potash brine-impacted groundwater: Built-in dual functions for desalination and pH neutralization. *Desalination* 419:141–151.

Paulchamy B, Arthi G, Lignesh BD (2015) A simple approach to stepwise synthesis of graphene oxide nanomaterial. *J Nanomed Nanotechnol* 6:1.

Rezaei-Aghdam E, Shamel A, Khodadadi-Moghaddam M, Ebrahimzadeh-Rajaei G, Mohajeri S (2022) Synthesis of a nanocomposite containing CTAB-stabilized Fe3O4 magnetic nanoparticles and a comparison between the adsorption behavior of cobalt ions on the nanocomposite and Typha latifolia L. *Theor Found Chem Eng.* 56:131–140.

Rostamian R, Heidarpour M, Mousavi SF, Afyuni M (2015) Characterization and sodium sorption capacity of biochar and activated carbon prepared from rice husk. *J Agric Sci Technol.* 17 (1-3): 1057–1069.

Sadeghi S, Albaji M, Golabi M, Ndnasab S Borooma (2022) Using modified natural zeolite clinoptilolite to remove nitrate, phosphate and salt from agricultural drainage water in a drainage system model. *Irrigation Sciences and Engineering (JISE)* 45:131–152.

Sasani M, Fataei E, Safari R, Nasehi F, Mosayebi M (2021) Antibacterial effects of iron oxide and silver nanoparticles synthesized by Bacillus subtilis: a comparative study. *Desalination and Water Treatment* 231:340–347.

Sherlala A, Raman A, Bello M, Asghar A (2018) A review of the applications of organo-functionalized magnetic graphene oxide nanocomposites for heavy metal adsorption. *Chemosphere* 193:1004–1017.

Solinska A, Bajda T (2022) Modified zeolite as a sorbent for removal of contaminants from wet flue gas desulphurization wastewater. *Chemosphere* 286:131772.

Ungureanu EL, Mocanu AL, Stroe CA, Panciu CM, Berca L, Sionel RM, Mustatea G (2023) Agricultural byproducts used as low-cost adsorbents for removal of potentially toxic elements from wastewater: a comprehensive review. *Sustainability* 5:5999.

Wang Y, Chen H, Liu Z, Li J, Tu Z, Li S (2023) Improved adsorption desalination performance of DUT-67 by incorporating Graphene Oxide (GO). *Microporous and Mesoporous Materials* 354 (1): 112554.

Wibowo E, Sutisna, Rokhmat M, Murniati R, Khairurrijal, Abdullah M (2017) Utilization of natural zeolite as sorbent material for seawater desalination. *Procedia Engineering* 170:8–13.

Wu H, Li L, Chang K, Du K, Shen C, Zhou S, Sheng G, Linghu W, Hayat T, Guo X (2020) Graphene oxide decorated nanoscale iron sulfide for highly efficient scavenging of hexavalent chromium from aqueous solutions. *J. Environ. Chem. Eng.* 8:103882.

Xu Z, Yan X, Du Z, Li J, Cheng F (2020) Effect of oxygenic groups on desalination performance improvement of graphene oxide-based membrane in membrane distillation. *Sep. Purif. Technol.* 251:117304.

Yusaf T, Mahamude ASF, Farhana K, Harun WSW, Kadirgama K, Ramasamy D, Kamarulzaman MK, Subramonian S, Hall S, Dhahad HA (2022) A comprehensive review on graphene nanoparticles: preparation, properties, and applications. *Sustainability* 14:12336.

Zaefizadeh M, Jalili A, Khayatnezhad M, Gholamin R, Mokhtari T (2011) Comparison of multiple linear regressions (MLR) and artificial neural network (ANN) in predicting the yield using its components in the hulless barley. *Advances in Environmental Biology* 5 (1): 109–114.

Zahed M, Parsamehr PS, Tofighy MA, Mohammadi T (2018) Synthesis and functionalization of graphene oxide (GO) for salty water desalination as adsorbent. *Chem Eng Res Des.* 138:358–365.

Zhang C, Li W, Liu C, Zhang C, Cao L, Kong D, Wang W, Chen S (2022) Effect of covalent organic framework modified graphene oxide on anticorrosion and self-healing properties of epoxy resin coatings. *Journal of Colloid and Interface Science* 608:10255–1039.